Raman microspectroscopy and imaging provides insights into heme aggregation and denaturation within human erythrocytes

Bayden R. Wood
Larissa Hammer
Lara Davis
Don McNaughton
Monash University
Centre for Biospectroscopy and School of Chemistry
Victoria 3800, Australia
E-mail: bayden.wood@sci.monash.edu.au

Abstract. The oxygenation process of a human erythrocyte is monitored using a Raman microimaging technique. Raman images of the 1638 cm^{-1} band are recorded in the oxygenated and deoxygenated state using only 120 s of laser exposure and ~1 mW of defocused laser power. The images show hemoglobin oxygenating and deoxygenating within the cell. Prolonged laser imaging exposure (<180 s) at low temperatures results in photoinduced and/or thermal degradation. The effect of thermal degradation is investigated by recording spectra of erythrocytes as a function of temperature between 4 and 52°C. Five bands at 1396, 1365, 1248, 972, and 662 cm^{-1} are identified as markers for heme aggregation. Raman images recorded of cells after prolonged laser exposure appear to show heme aggregation commencing in the middle and moving toward the periphery of the cell. UV-visible spectra of erythrocytes show the Soret band to be broader and red shifted (~3 nm) at temperatures between 45 and 55° indicative of excitonic interactions. It is postulated that the enhancement of the aggregation marker bands observed at 632.8-nm excitation results primarily from excitonic interactions between the aggregated hemes in response to protein denaturation. The results have important medical implications in detecting and monitoring heme aggregation associated with hemopathies such as sickle cell disease. © *2005 Society of Photo-Optical Instrumentation Engineers.* [DOI: 10.1117/1.1854678]

Keywords: resonance Raman spectroscopy; Raman imaging; red blood cell; hemoglobin; aggregation; excitonic coupling.

Paper 03144 received Dec. 2, 2003; revised manuscript received May 5, 2004; accepted for publication Jun. 15, 2004; published online Feb. 8, 2005.

1 Introduction

An important indicator of disease or dysfunction in an erythrocyte is the O_2 storage capacity. Current dioxygen (O_2) determination is only carried out on bulk cells to determine an average cell concentration, while individual cell O_2 concentrations that can be correlated with the health/viability of the individual cells are really required. Information from single cells provides insights into the heterogeneity of the total cell population and a means to ascertain variability within that population. Raman spectroscopy has already proven to be a powerful technique to monitor the molecular dynamics of the R (relaxed with a higher O_2 concentration) to T (tense with lower O_2 concentration) of hemoglobin (Hb).[1] Early reports using Hb solutions by Spiro and Streakas,[2] and Brunner, Mayer, and Sussner[3] demonstrated the sensitivity of the technique in the detection of heme perturbation resulting from Fe displacement from the porphyrin plane. In the deoxygenated state, the Fe atom is in a ferrous high spin state ($S = 2$) and lies approximately 0.4 Å out of the porphyrin plane.[4] In the oxygenated state, the Fe atom is in a ferrous low spin state

($S = 0$) and resides much closer to the plane. The binding of O_2 to the sixth coordination position of the Fe atom triggers a biochemical cascade that characterizes the T to R state transition. As the Fe atom moves into the porphyrin plane, it essentially pulls the proximal F8 histidine coordinated to the Fe in the fifth position, which shifts the F helix.[5] The resulting conformational change is transmitted to the subunit interfaces, breaking salt bridges between terminal amino acid groups on the subunits and leading to the T-to-R state transition. Consequently, O_2 binding at one heme site is communicated to neighboring heme sites.[5]

UV resonance Raman studies investigated the role of aromatic amino acid residues in the T-to-R state transition. By selectively enhancing tyrosine and tryptophan residues of mutant Hbs using 200- and 212-nm excitation, dramatic band shifts and intensity enhancement were observed between the two quaternary states.[6] These alterations were attributed to the formation and destruction of hydrogen bonds and demonstrated which tyrosine residues are involved in the T-to-R state transition.[6] While the molecular dynamics of the allosteric transition in Hb have been extensively studied in solu-

Address all correspondence to Donald McNaughton, Monash Univ., Melbourne, Australia. E-mail: Don.McNaughton@sci.monash.edu.au

tion, few studies have focused on the nature of this transition within the red blood cell.

Raman microspectroscopy has proven to be an ideal tool to detect and monitor heme groups within single cells. The Raman confocal technique has found application in monitoring myeloperoxidase in living neutrophils[7] and eosinophil peroxidase in living eosinophilic granulocytes.[8] The technique was used to detect intracellular NADPH-oxidase activity in neutrophilic and eosinophilic granulocytes following mitogenic stimulation.[9] Raman imaging, on the other hand, can provide information on the spatial distribution of molecules within cells.[10] Ramser, Fant, and Käll[11] reported effects that influenced Raman images and spectra of single functional erythrocytes using 514-nm excitation. These included changes in the cell membrane due to a surface-induced effect possibly mitigated by the poly-L-lysine used to attach the cells, and a photoinduced fluorescence effect possibly resulting from the conversion of oxyHb to metHb. The fluorescence effect masked any chance of obtaining reliable images of cells in the oxygenated and deoxygenated state.[11]

Our initial work focused on the Raman characterization of the T-to-R state transition of Hb within a functional single red blood cell (RBC) using 632.8-nm excitation.[12] Erythrocytes immersed in phosphate buffered saline were affixed by poly-L-lysine to an aluminum coated Petri dish and spectra recorded using a water immersion objective. Cells were deoxygenated by passing N_2 over the suspension and reoxygenated by exposing the suspension to atmospheric O_2. In one study,[13] spectra were recorded at 1-min intervals and processed with a principal components (PC) analysis. The PC1 scores plot exhibited a sigmoidal curve, which was the reciprocal of the percent of O_2 saturation versus the partial pressure curve normally observed in hemoglobin solutions.[5] The inflection point on the curve correlates to the T→R state transition point. Consequently, it was possible to identify and characterize spectra of totally oxygenated and totally deoxygenated cells as well as examine the spectrum corresponding to the transition point.[13] The transition point spectrum exhibited spectral features indicative of both oxygenated and deoxygenated states as expected from a cell containing Hb with varying degrees of oxygenation.[13] At 632.8-nm excitation, thermal degradation and cell damage are minimized and the spectra have excellent signal to noise. All bands observed at this excitation wavelength are essentially from the heme group, with little or no contribution from the protein or other cellular macromolecules. By comparing spectra of the cells in both the oxygenated and deoxygenated states with heme derivatives such as hemin, hematin, and HbA_1, along with cells containing methemoglobin (metHb) and carboxy-Hb, it was shown that the major differences between the oxygenated and deoxygenated states reflected changes in the spin states of the Fe atoms.[12] The change in spin state is accompanied by dramatic heme perturbation as the Fe atom translocates in and out of the porphyrin plane. This heme perturbation is characterized by the porphyrin core deforming and possibly ruffling to accommodate the Fe atom as it descends into the porphyrin plane on binding to O_2.[14] Consequently, the bond lengths and angles are modified, which in turn is detected with the Raman technique. In previous publications we have shown unusual band enhancement occurring at 632.8 nm, where no obvious electronic transition is observed in oxyRBCs. It is possible that preresonance with the Q_0 band accounts for the enhancement at 632.8-nm excitation, but a Raman excitation profile recorded in 10-nm intervals from 573 to 633 nm of crystallized HbA_0 clearly showed the enhancement at 633 nm to be independent of resonance or preresonance Raman scattering from the Q_0 band.[12] This enhancement enables high-quality Raman spectra of erythrocytes to be obtained at the 632.8-nm excitation wavelength.

We present Raman images of functional erythrocytes in both the oxygenated and deoxygenated state. The effects of thermal denaturation and photoinduced damage are investigated by recording spectra of cells as a function of temperature and laser exposure. It is hypothesized that the unusual Raman profile of erythrocytes at temperatures greater than 42°C and/or after prolonged laser exposure results from excitonic effects as a consequence of heme aggregation in response to thermal denaturation and/or photoinduced degradation of the Hb. The study provides a methodology and approach to ensure that images of erythrocytes are true Raman images and not the result of heme aggregation in response to protein denaturation.

2 Experiments

2.1 Erythrocyte Preparation

Blood (1 cm^3) was obtained by venipuncture from healthy volunteers and placed in glass tubes containing acid citrate dextrose as an anticoagulant. The blood was centrifuged (2200 rpm for 5 min) to produce a buffy coat. A 20-μL aliquot of blood collected from underneath the white blood cell layer was diluted to 10 cm^3 with phosphate buffered saline (PBS) at 25°C. Cells were transferred to a 80-mm-diam glass Petri dish sputter coated with aluminum. The Petri dish was further coated with 0.01% poly-L-lysine hydrobromide [SIGMA (Clayton, Victoria, Australia), mol. weight between 70,000 and 15,000 Kda] solution and dried with a hair dryer prior to the addition of the suspension. The Petri dish was placed into a temperature-controlled cell (Physitemp™, TS-4LPD, large Petri dish stage) with a TS-4 thermoelectric controller (Physitemp™, Clifton, New Jersey). A Perspex lid was developed to enclose the Petri dish and seal the water immersion objective from the atmosphere. The lid had inlet and outlet pipes for gas exchange, along with inlet holes for temperature and pH probes. Figure 1 depicts a schematic of the purpose-built Raman cell for the analysis of single cells, along with a photograph of the device on the temperature-controlled translation stage. The cells were allowed to settle (~10 min) before spectra were recorded.

2.1.1 MetHb erythrocytes

The metHb RBCs were prepared by resuspending washed RBCs in 0.1% sodium nitrate solution and leaving the suspension to stand for 1 h at room temperature. The cells were washed a further three times in 0.9% saline prior to analysis. The conversion of oxy to metHb RBCs was confirmed by UV-visible spectroscopy that clearly shows the 635-nm band, which is indicative of the metHb formation.
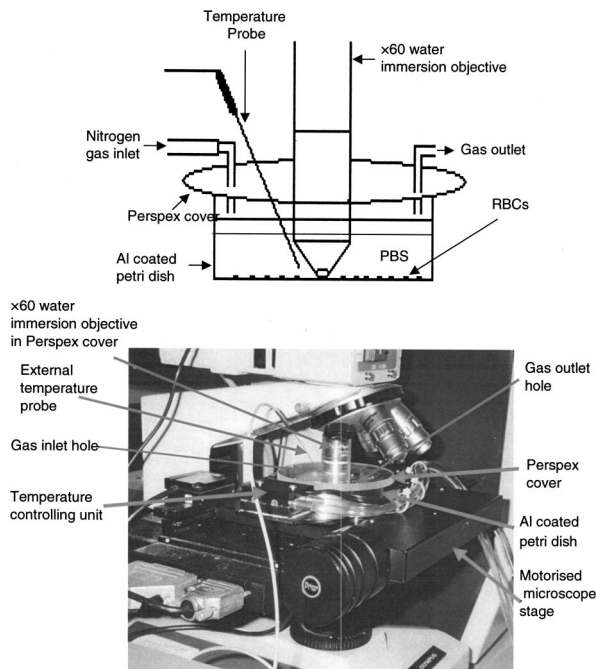
Fig. 1 (top) Schematic of purpose-built Raman cell for single red blood cell analysis. (bottom) Photograph showing positioning of Raman cell mounted on the Physitemp™ temperature control unit and placed in position on the microscope stage.

2.2 Single Crystal Preparation

MetHb monoclinic crystals and oxyHb orthorhombic crystals were prepared using the method of Drabkin.[15] Briefly, 4 ml of packed red cells were isolated from fresh human blood collected in acid citrate dextrose heparinized tubes and washed three times in 0.9% saline. The metHb cells were resuspended in 0.1% sodium nitrate solution and left to stand for 1 h at room temperature before being washed a further three times in 0.9% saline. For both oxyHb and metHb cells, stroma free solutions (~8 to 10 mM) were prepared by dilution with 4 ml of distilled water and 0.4 ml of toluene, followed by thorough mixing, overnight refrigeration, and siphoning off of the clear layer of Hb. The Hb solutions were then dialyzed against $(NH_4)_2SO_4$ (700 gm plus 1 L of water) by transferring ~2-ml Hb solutions into dialysis tubing (Visking size 2-18/32″ Medi-cell International Limited) and leaving the Hb solution in the tubing until the volume reduced by approximately 45%. The Hb supernatant was then approximately 14 to 17.5 mM by titer.[15] Crystallization was accomplished by adding several drops of concentrated $(NH_4)_2SO_4$ and monitoring the crystal formation with the microscope.

2.3 UV-Visible Spectroscopy

Absorption spectra (350 to 650 nm) measurements were measured with a Cary 5000 UV-visible spectrometer coupled with a temperature control accessory. The measurement parameters were set to 0.4-nm bandwidth, 1-s integration time, 40 nm/min scan speed, and data were recorded at 0.4-nm intervals. 10 μL of packed washed red cells were resuspended in 10 ml of 0.9% saline. Approximately 2 ml of suspended red cells were placed in a quartz cuvette. A second quartz cuvette was filled with 0.9% saline and served as a background. Spectra

were recorded as a function of temperature between 25 to 65° in 5° intervals with slow stirring. At each 5° interval, three spectra were recorded in the 350- to 650-nm region. A similar experiment was also performed on isolated Hb that was prepared by lysing 10 μL of red cells in 10 ml of distilled water. To enable direct comparison, spectra were baseline corrected with three points (360, 460, and 600 nm) and min/max normalized to the Soret band using OPUS™ spectroscopic software.

2.4 Raman Spectroscopy and Imaging

Raman spectra of functional erythrocytes were recorded on a Renishaw system 2000 (Renishaw plc, Wootton-under-Edge, Gloucester, UK) using a 632.8-nm excitation line from a He-Ne laser and equipped with a modified BH2-UMA Olympus optical microscope (Olympus Australia, Mt. Waverly, Victoria, Australia) and water immersion objective (Zeiss, 60×, numerical aperture 0.9). Spectra were recorded between 1800 and 300 cm^{-1} with a resolution of *ca* 1 to 2 cm^{-1}. The 520.5-cm^{-1} band of a silicon wafer was used to calibrate the instrument on a daily basis. Unless otherwise stated, all spectra presented were recorded using 10 s of laser exposure with 1 scan accumulation. In all experiments, the laser power was kept constant at 2.0±0.1 mW for a 1- to 2-μm laser spot size. Spectra were baseline corrected and cosmic ray signals removed in OPUS™ Spectroscopic Software (Bruker Optics, Karlsruhe, Germany) and GRAMs spectroscopic software, respectively.

Raman images were recorded with the laser defocused to ~15 μm to encapsulate the cell. Before image collection, the image filter was calibrated to the band of interest by recording a spectrum across the filter and comparing the result with a normal Raman spectrum of the cell. The filter image was offset corrected by approximately 20 cm^{-1}. After each image was recorded, normal Raman spectra were acquired (1 accumulation, 10-s exposure) to assess the effects of laser exposure. Two types of Raman imaging experiments were performed to investigate the effects of prolonged laser exposure and thermal effects. The Raman parameters and methodology for these experiments are given in the next section.

2.5 Oxygenation and Deoxygenation Experiments

Deoxygenation was achieved by equilibrating the erythrocyte suspension with nitrogen. This was achieved by passing N_2 gas over the top of the suspension (5 cm^3 per min) through the inlet and outlet holes in the Perspex Petri dish lid of the purpose-built Raman cell. Oxygenation was achieved by stopping the N_2 flow and allowing the system to equilibrate with atmospheric O_2. Seven experiments that entailed recording Raman spectra and/or images at various times and temperatures during the oxygenation and deoxygenation process were performed in duplicate or triplicate.

Raman spectra on oxygenation/deoxygenation

With the temperature held constant at 4°C, N_2 gas was passed over the suspension for 20 min. Spectra were recorded at 5-min intervals during this interval during this deoxygenation process. The suspension was then allowed to equilibrate with atmospheric O_2 and spectra were recorded at the 25 and 30 min mark. MetHb erythrocytes were prepared by immersing

10 μL of washed erythrocytes into a 0.1% solution of sodium nitrite made up to 10 cm^3 with PBS. The erythrocytes were incubated for one hour at room temperature prior to deposition onto the Petri dish and spectra were recorded as described earlier.

Raman images on oxygenation/deoxygenation

Raman images were collected at 10-min intervals for 50 min from a single cell deoxygenated under N$_2$ flow at room temperature. The N$_2$ flow was then turned off and images of the same cell were recorded every 10 min from the 60- to 90-min mark as the cell gradually oxygenated. For each image, the laser was defocused to the size of the erythrocyte and the image was collected with 180 s of continuous laser exposure. A Raman spectrum was recorded immediately following each image acquisition.

Raman spectra as a function of temperature

Raman spectra of single erythrocytes were recorded as a function of temperature in the oxygenated state. Spectra were recorded every 4°C (± 0.1°C) from 4 to 52°C as measured with the Physitemp™ microprobe, with the probe tip located ~2 mm from the cell. Spectra were baseline corrected and plotted in a 3-D matrix plot using the Statistica™ software package.

Raman spectra as a function of temperature cycling

Raman spectra were recorded of a single cell in a suspension at 4°C, 42°C, and again on recooling to 4°C.

Effects of laser exposure

To test the effect of continuous laser exposure, a fresh suspension of cells was cooled to 4°C. A single cell was exposed to the laser light for 3 min, and a spectrum was recorded. The cell was allowed to relax without any laser exposure for 15 min before another spectrum was taken. A third spectrum was recorded 2 h after the initial laser exposure. These spectra were compared to assess the long-term effects of extended laser exposure.

Raman images under reduced power flux

Raman images of a single cell were recorded on the same cell at 4°C with only 120 s of constant laser exposure per image. Only three images were recorded (every 40 min for 120 min) in the deoxygenated, oxygenated, and deoxygenated states on the same cell. Power at the sample was set to 50% of full power, i.e., ~1 mW.

Power dependence study

In the final experiment, erythrocytes were cooled to 4°C and Raman spectra were recorded as a function of power using a set of neutral density filters. For each power measurement, five spectra were recorded from five different erythrocytes. The power dependence experiment was also repeated at 42°C. To ensure that observed changes were not the result of instrumental artifacts, a power-dependence profile of the silicon band at 520.5 cm^{-1} at room temperature was also recorded.

3 Results

3.1 Electronic Absorption Spectroscopy

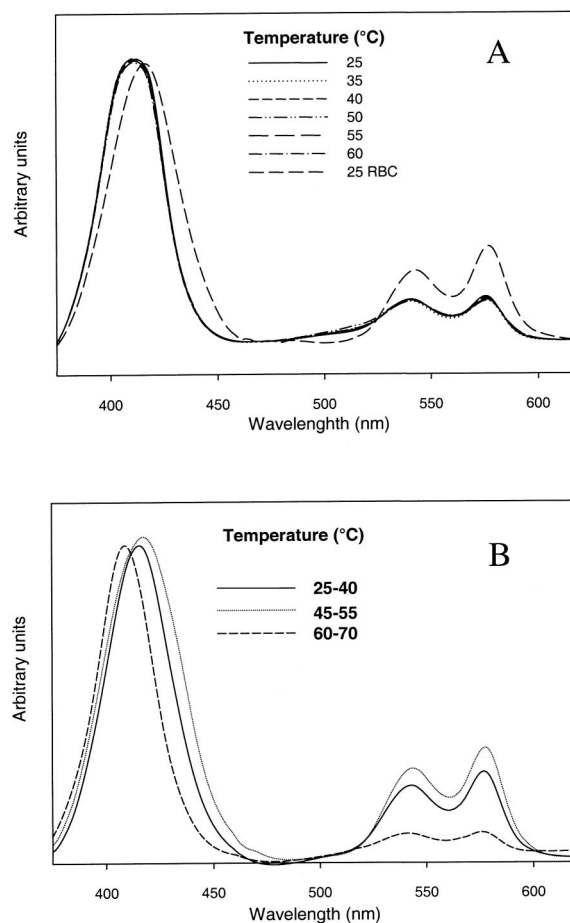Figure 2(a) shows ultraviolet-visible spectra of isolated Hb

Fig. 2 (a) Absorption spectra of hemoglobin recorded as a function of temperature at 632.8-nm excitation. Spectra were acquired in 5°C intervals from 25 to 60°C. The spectrum of red blood cells recorded at 25°C is plotted on the same plot for comparison. (b) Absorption spectra recorded of intact red blood cells as a function of temperature. For clarity the spectra have been grouped in ranges of 25 to 40°C, 45 to 55°C, and 60 to 70°C.

recorded from 25 to 60°C in 5°C intervals, and a spectrum of red blood cells recorded at 25°C. The absorbance spectra of the isolated Hb are virtually identical for the entire temperature range. These spectra differ significantly in terms of relative band intensity, band width, and position compared to the spectrum of the red cells recorded at 25°C. The full-width-half-maximum of the Soret band (~416 nm) is considerably greater in the red cells and is red-shifted 3 nm. The ratio of the Q$_0$ band to the Soret band in RBCs is larger than in isolated Hb. Figure 2(b) depicts UV-visible spectra of RBCs as a function of temperature. Spectra were recorded every 5°C from 25 to 65°C. For clarity, the spectra presented have been grouped into three temperature intervals 25 to 40°C, 45 to 55°C, and 60 to 65°C. UV-visible spectra recorded of RBCs in the 45 to 55°C range clearly show broadening and a red shift (~3 nm) of the Soret band compared to spectra recorded in the physiological tolerant temperature region (25 to 40°C). The Q bands are also slightly broader and red shifted (1 to 2 nm) at the higher temperature. At 55°C, the cells start to lyse, releasing Hb into the saline. The free denatured Hb causes a
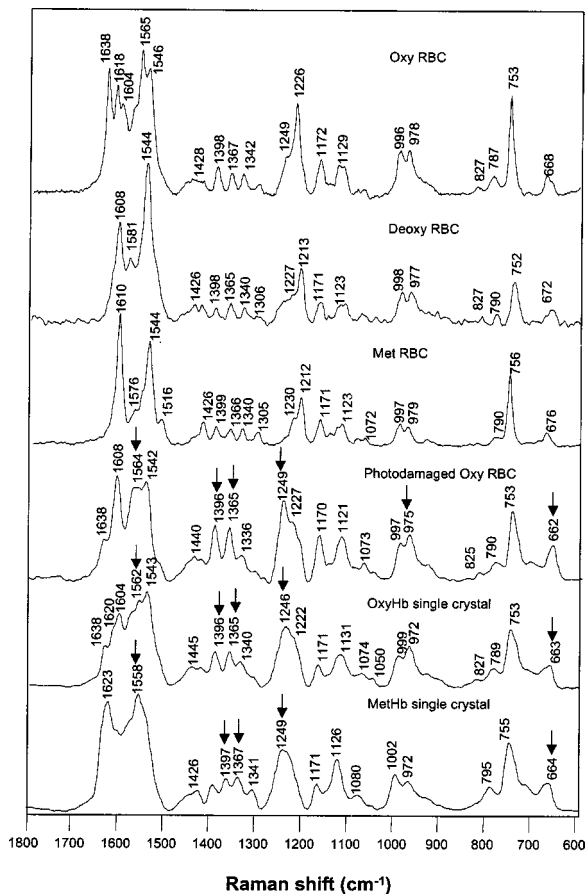
Fig. 3 Raman spectra of oxygenated, deoxygenated, and metHb-erythrocytes recorded at 4°C along with a spectrum of a photodamaged cell and spectra of crystallized oxyHb and metHb, all recorded with 632.8-nm excitation (10-s laser exposure, one accumulation).
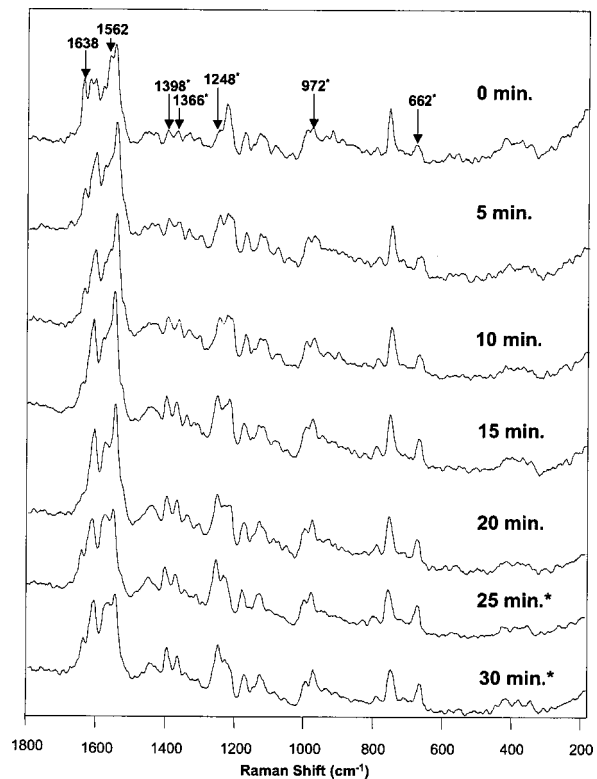

Fig. 4 Raman spectra recorded of an oxygenated cell gradually deoxygenated (0 to 20 min) and then reoxygenated (25 to 30 min). The asterisks show the bands that appear to increase due to constant laser exposure, while the other named bands follow the oxygenation cycle of the cell.

dramatic blue shift and narrowing of the Soret band, and the Q bands are considerably weakened at these very high temperatures.

3.2 Raman Spectroscopy and Imaging

Figure 3 depicts Raman spectra of oxygenated, deoxygenated, metHb-erythrocytes recorded at 4°C with one accumulation and 10 s of laser exposure. The figure also shows a spectrum of a red cell recorded after 200 s of intermittent focused laser exposure along with spectra of recrystallized metHb and oxyHb crystals. The minimal laser exposure, long resting time between measurements, and low temperature of the suspension minimizes thermal denaturation and photodegradation. The spectra of the fully oxygenated and deoxygenated cells are similar to those previously reported by our group at room temperature.[12,13,16] In the oxygenated state, the 1500 to 1650 cm^{-1} region has a profile consistent with the heme Fe atom in a low-spin state ($S=0$) with bands at 1638, 1618, 1604, 1582 (shoulder), 1565, and 1546 cm^{-1}.[12] The 1638-cm^{-1} band is known as a marker band for O_2 concentration. In the deoxygenated state, this region has three dominant bands at 1608, 1581, and 1544 cm^{-1}, consistent with the Fe atom in the high-spin ($S=2$) state.[12] The band at 1226 cm^{-1} appears to shift to 1213 cm^{-1} in the deoxygenated cell. The spectrum of the metHb-erythrocyte is similar to the spectrum of the

deoxygenated cell, especially in the 1620- to 1500-cm^{-1} region showing a characteristic three-band profile indicative of high-spin heme complexes. Differences between met and deoxy erythrocytes include the increase in relative intensity of the 1610-cm^{-1} band and the enhancement of the 1516-cm^{-1} shoulder band. The spectrum of the cell following prolonged laser exposure has a number of characteristic features that distinguish it from the other cell types. These include the dramatic increase in the relative intensity of bands at 1396, 1365, 1248, 972, and 662 cm^{-1}. It is important to note that these bands also appear enhanced in the single crystal spectra for both oxyHb and metHb.

Figure 4 depicts a time series of spectra of erythrocytes gradually deoxygenating in the first 20 min and then reoxygenated from this point onward. Spectra were recorded at 5-min intervals using minimal power (25% of the initial power) and at 4°C. The spectra show the dioxygen marker band (v_{10}) at 1638 cm^{-1} clearly decreasing during deoxygenation and then rapidly increasing when the cell suspension is exposed to the atmospheric dioxygen. The intensity of the totally symmetric A_{1g} mode at 1564 cm^{-1} assigned to v_2 also appears to cycle with O_2 concentration. Other bands, including the pyrrole in-phase breathing modes at 1396 and 1365 cm^{-1} along with the methine deformation mode at 1249 cm^{-1} and bands at 975 and 662 cm^{-1}, increase during the entire experiment, indicating a photoinduced effect caused by multiple spectral acquisitions on the same cell.
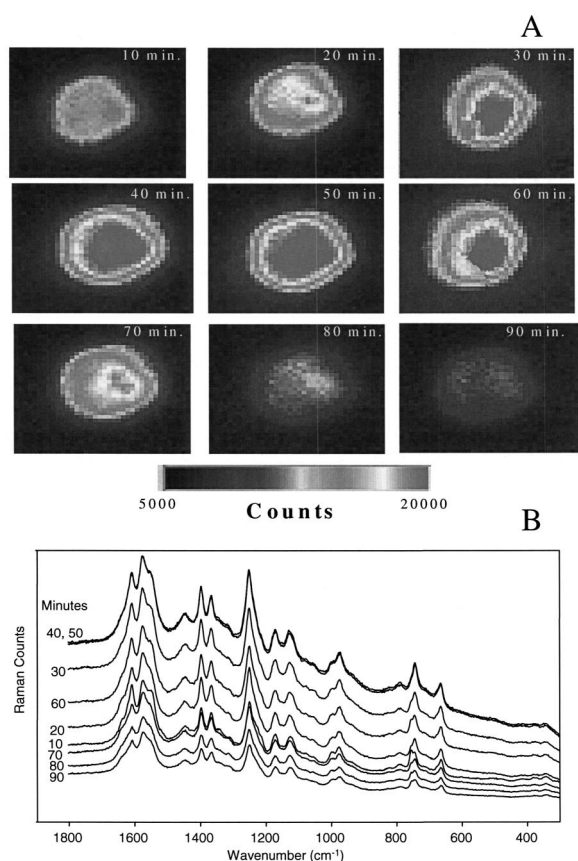
Fig. 5 (a) Raman images of the 1250- to 1210-cm^{-1} region recorded on the same cell during deoxygenation (0 to 50 min) followed by reoxygenation (50 to 90 min) using 632.8 nm. Each image was acquired with 180 s of continuous defocused laser exposure. (b) Corresponding Raman spectra recorded after each image presented in (a).

Figure 5 depicts a time series of Raman images centered on the 1249-cm^{-1} band of a single erythrocyte gradually deoxygenating to 50 min because of nitrogen exchange. The cell is then reoxygenated by exposure to atmospheric O_2. The 1249-cm^{-1} band was chosen as the imaging band because of its radical intensity change from constant exposure. Based on the filter bandpass, the actual wavenumber region imaged was found to be approximately 20 cm^{-1}. Each image was recorded at room temperature by defocusing the laser to encapsulate the cell and acquiring the image with 180 s of constant laser exposure. The first image recorded after 10 min of deoxygenation shows a homogenous green background. The intensity of counts increased as the cell became more deoxygenated with continuous laser exposure. After 50 min the cell is completely deoxygenated and the image is bright red, indicating a high number of Raman counts. Figure 5 also shows the corresponding Raman spectra collected directly after each image was recorded. The raw spectra show a marked increase in both the baseline and enhancement of many bands as the cell deoxygenates. At the 50-min mark, the cell is reoxygenated and the subsequent images from the 60-min mark to 90 min show a decrease in the overall band intensities and baseline. However, the actual relative intensities do not change from the deoxygenated to the oxygenated state, and the spectra do not resemble those of the oxygenated cell depicted in Fig. 2.

Small spectral changes were observed in the 755- to 745 and 1650- to 1500-cm^{-1} region. In particular, the bands at 755 cm^{-1} and 1638 cm^{-1} appear to follow the oxygenation-deoxygenation cycle.

To investigate the origin of this phenomenon, spectra of erythrocytes were recorded every 2°C from 4 to 52°C. Five spectra were recorded from five different cells at 4°C intervals. The spectra were averaged and then baseline corrected using eight baseline minima points. Figure 6 depicts baseline-corrected interpolated matrix plots of different spectral windows showing the Raman counts as a function temperature. Due to laser exposure, the actual temperature of the cell would be a few degrees higher than that recorded by the probe, which is ~2 mm from the cell. This approximation is based on the calculations and approximations by Ramser, Fant, and Käll.[11] At the higher temperatures (<42°C), the spectra are very similar to the spectra presented in Fig. 5(a), which were recorded after sustained laser exposure resulting from multiple Raman images recorded from the same cell. The spectra exhibit dramatic changes in band intensity as the temperature increases. Bands at 1609, 1398, 1366, 1250, 1170, 1123, 998, 972, and 666 cm^{-1} increase, while bands at 1638, 1565, 1621, and 1226 cm^{-1} decrease in intensity. As the temperature increases, so to does the signal-to-noise ratio (SNR). Figure 7 depicts a plot of signal to noise for the 1250- to 1200-cm^{-1} (signal) and 1800- to 1700-cm^{-1} (noise) region at each temperature. The SNR measurements were calculated using the SNR function based on the root mean square of deviations (i.e., standard deviation) in OPUS™ spectroscopic software from five spectra recorded from five separate cells at each temperature. The SNR values were averaged for each temperature and plotted as a function of temperature. The line through the points indicates the general trend, which shows the SNR gradually increasing as the temperature increases.

As noted before, the spectra in Fig. 6 closely match those presented in Fig. 5. Consequently, the images presented in Fig. 5 and the corresponding spectra reflect spectral changes that accompany denaturation of the Hb. The fact that oxygenation appears to reduce the SNR can be explained in terms of excitonic interactions, as is discussed later. To further investigate the effects of thermal denaturation, a suspension of cells was cooled to 4°C and a spectrum recorded of a single cell. Further spectra of the same cell were recorded after first warming the suspension to 42°C and then cooling to 4°C; they are presented in Fig. 8(a). The top spectrum closely matches the bottom spectrum and is characteristic of oxyHb, while the middle spectrum is a close match to spectra recorded at high temperatures and/or after continuous laser exposure, proving that the thermal denaturation effect can be reversed if the damage is not too severe. Moreover, this result conclusively demonstrates that the spectrum that characterizes the thermal and/or photodamaged cell with enhanced bands at 1396, 1365, 1248, 972, and 662 cm^{-1} is not metHb simply because metHb cannot be converted back to oxyHb. The effects of laser exposure were investigated by exposing the cell to continuous laser exposure at a low temperature for 3 min at 4°C before recording a spectrum. Spectra were then recorded at 15 and 120 min after the laser exposure. The resultant spectra, shown in Fig. 8(b), show that the change induced by constant laser exposure is irreversible. The spectra are a close match to those recorded following the 180-s image acquisi-
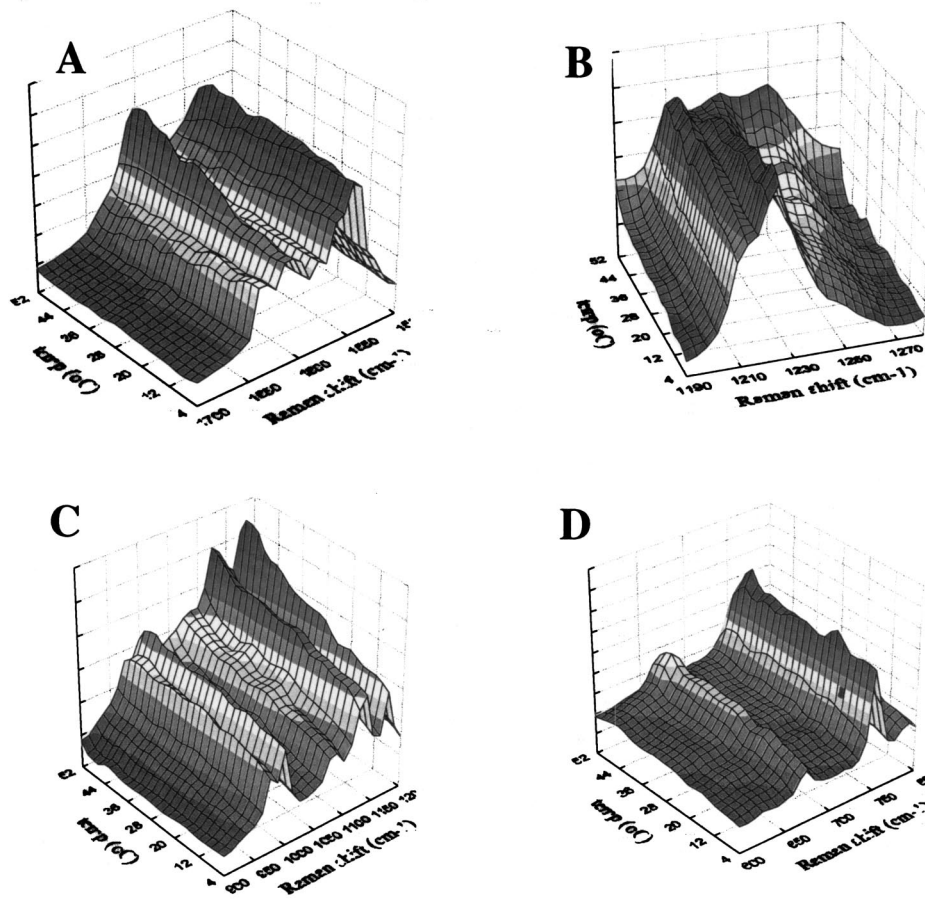
Fig. 6 Interpolated plots showing baseline corrected Raman spectra as a function of temperature for the (a) 1700 to 1500, (b) 1270 to 1190, (c) 1200 to 900, and (d) 800 to 600 cm^{-1} regions.
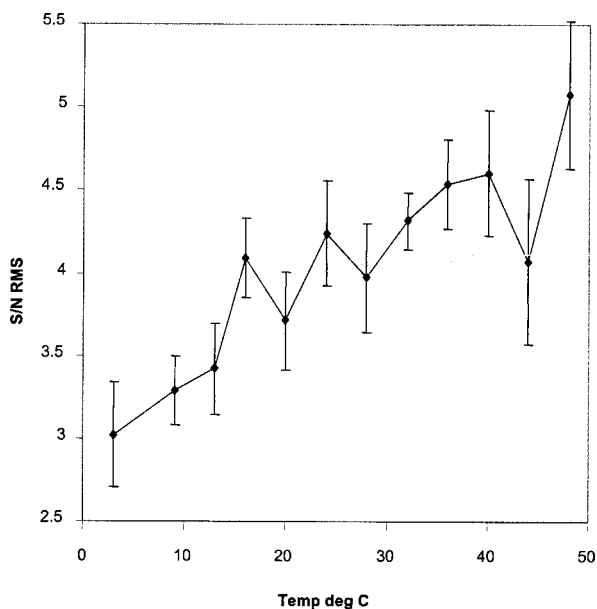

Fig. 7 A plot of the signal-to-noise ratio for the 1250 to 1200 cm^{-1} (signal) and 1800 to 1700 cm^{-1} (noise) region at specified temperatures.

tions presented in Fig. 5 and the thermally affected cells presented in Fig. 6.

The effects of thermal degradation and photoinduced degradation were minimized by reducing the temperature of the solution to 4°C and recording only three images per cell over a 120-min period (i.e., one image every 40 min). Each image was recorded using only 120 s of constant laser exposure rather than 180 s. Figure 9 depicts Raman images, centered on the 1638-cm^{-1} band, of a single erythrocyte initially deoxygenated and then oxygenated. The 1638-cm^{-1} band was chosen because of its radical change during deoxygenation, as shown in Fig. 3. We previously established that cells are totally oxygenated after 20 min using this approach.[13] The image at 20 min therefore represents the cell fully oxygenated. The 1638-cm^{-1} images appear to show the cell oxygenating and deoxygenating. The blue areas on the image represent low O$_2$ concentration, while the red indicate high O$_2$ concentration. This image totally contrasts the corresponding image at 90 min in Fig. 5, which shows the fully oxygenated erythrocyte predominantly blue. The corresponding spectra recorded immediately after each image are also depicted in Fig. 9. The spectra of the oxygenated and deoxygenated erythrocyte in Fig. 8 are a good match to the corresponding spectra presented in Fig. 2 and show minimal effects due to thermal denaturation. In this case, the background contribution to the baseline is minimal; consequently, these can be regarded as
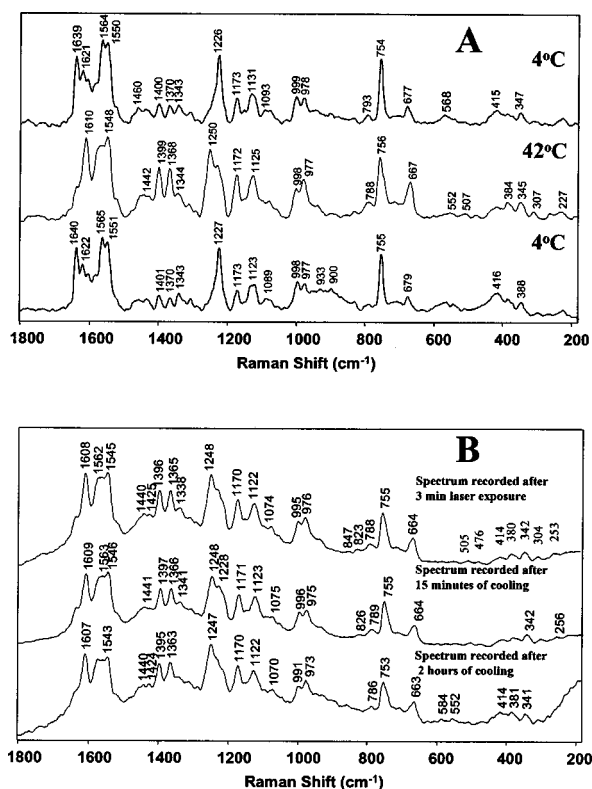
Fig. 9 Two Raman images recorded on the same cell, (a) deoxygenated and (b) oxygenated. Each image was recorded at 4°C with only 120 s of constant laser exposure and 40 min rest between images.

Fig. 8 (a) Raman spectra recorded of a single cell in sequence, first at 4°C, heated to 42°C, then cooled again to 4°C. Each spectrum was recorded at the center of the cell with 10 s of focused laser exposure and only one accumulation. The thermal changes in the spectrum are shown to be reversible. (b) Raman spectra recorded of a single cell in sequence. Cell was cooled to 4°C and exposed to 100% laser power for 3 min. The cell was then allowed to cool and spectra were taken after 15 min and 2 h. Each spectrum was recorded at the center of the cell with 10 s of focused laser exposure and one accumulation. In this case, the induced effect was irreversible.

true Raman images and not the result of thermal or photoinduced denaturation of Hb.

We hypothesized that the anomalous enhancement of numerous bands in the spectra of red cells at high temperatures and/or prolonged laser exposure results from strong excitonic interactions between aggregated heme moieties. To test this hypothesis, a power-dependence study was performed on cells at 4 and 42°C, respectively. For normal Raman enhancement there is a linear relationship between power and the intensity of Raman bands. However, when there are excitonic interactions, a nonlinear relationship between power and band intensity is predicted. Excitonic interactions are expected in the erythrocyte due to the closely packed arrangement of Hb enabling energy in the form of an exciton to migrate throughout the cell. Figure 10 depicts the power dependence of the 520.5-cm^{-1} band of silicon along with the power dependence of a number of bands from the heme moiety in the red blood cell at 4 and 42°C. As expected, the silicon mode clearly shows a linear dependence as a function of power. However, both the 4 and 42°C power-dependence measurements on Hb within the erythrocyte show a nonlinear dependence. Moreover, the enhancement of vibrational modes as a function of power is greater at 42 than 4°C and appears to reach a satu-
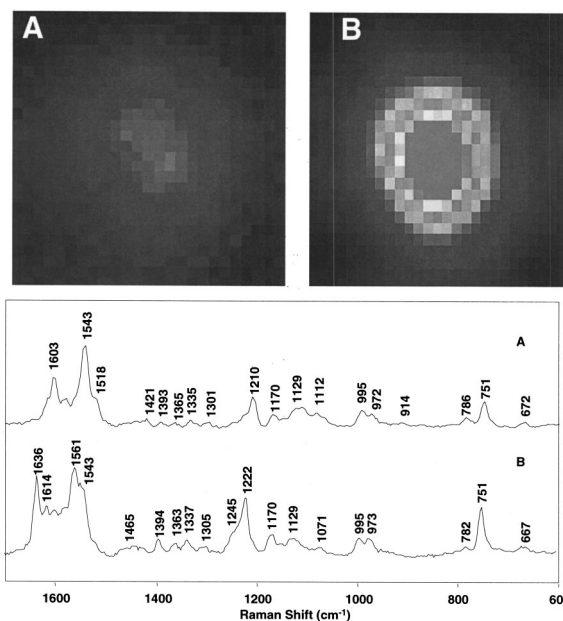
ration point at 80% power for some bands at the higher temperature.

3.3 Discussion

By applying 632.8-nm excitation, high-quality Raman images of single erythrocytes undergoing oxygenation and deoxygenation can be acquired if the effects of thermal degradation and photodegradation are minimized. In the current study this was achieved by reducing the temperature of the suspension, reducing the exposure time of the laser, reducing the laser power, and limiting the number of multiple images acquired per cell. Using this conservative approach, most of the cells retain their discoid morphology and there is no evidence of Heinz bodies. The majority of cells can remain affixed to the Petri dish for up to three hours when placed in temperature-controlled buffered growth media without any change to morphology or accumulation of Heinz bodies, even after 2×120 s of laser exposure (40 min apart). To determine whether or not the images recorded are true Raman images and not the result of protein denaturation or some other degradation process, it is essential to record spectra directly after each image. Spectra recorded following multiple imaging and prolonged laser exposure on the same cell showed evidence of heme aggregation in response to photoinduced denaturation of Hb. The spectral changes associated with heme aggregation include an increase in signal to noise, dramatic enhancement of many bands, and a general increase in background counts. At high temperatures ($<42°C$), the proteins within the cell naturally start to denature. Hb denaturation is accompanied by aggregation of the heme moieties. The aggregation is facilitated by the extremely high concentration of Hb within the red blood cell, which is ~ 22 mM.[17] Spectra recorded of a single cell undergoing oxygenation/deoxygenation enabled the identification of vibrational modes that become enhanced when hemes aggre-
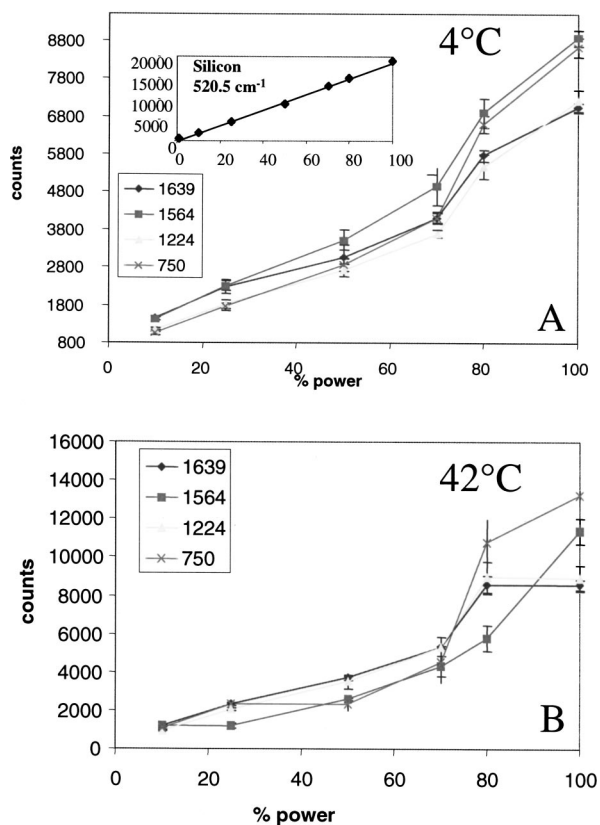
Fig. 10 Plots showing Raman counts for a number of selected bands as a function of power and temperature. (a) Plot of Raman counts versus power at 4°C. Inset shows power-dependence study of the 520.5-cm^{-1} silicon band at room temperature. (b) Corresponding plot at 42°C.

gate. These include bands at 1396, 1365, 1249, 972, and 662 cm^{-1}. The 1396 and 1365 cm^{-1} bands are assigned to pyrrole in-phase breathing vibrations, while the 1248-cm^{-1} mode is assigned to a methine deformation mode. We suggest all these bands are marker bands for heme aggregation as they continue to become enhanced at high temperatures and/or after prolonged laser exposure. The appearance of heme aggregation bands along with the O$_2$ marker band at 1638 cm^{-1} indicates that the cell contains a mixture of functional Hb and aggregated heme. Multiple Raman images recorded on the same cell with 180-s laser exposure at room temperature enabled us to visualize the aggregation process. The hemes appear to initially aggregate within the center of the cell, with the aggregate increasing in size and gradually occupying the entire cell.

It is hypothesized the spectral changes observed in red cells at high temperatures and/or after prolonged laser exposure result from excitonic interactions between the metalloporphyrins as a consequence of heme aggregation in response to Hb denaturation. On aggregation, the intermolecular distance between heme groups within the cell dramatically decreases. This facilitates migration of energy in the form of an exciton throughout the porphyrin network. The multiple Raman images and subsequent spectra recorded on the same cell after prolonged laser exposure revealed a number of interesting observations. First, there is a general decrease in

background and band intensity on reoxygenation. It is important to note that while the overall band intensity and background decreased on reoxygenation, the relative band intensities remained essentially unchanged for the majority of bands. Moreover, the band thought to be an indicator of O$_2$ concentration, assigned to v_{10} at 1638 cm^{-1}, appears relatively unchanged, indicative of Hb dysfunction. It is possible that O$_2$ is still binding to the Fe center, just not cooperatively, or alternatively that the O$_2$ molecule is behaving as an "intermolecular spacer." In this case, the O$_2$ molecule may create distance between the aggregated porphyrins, thereby reducing the excitonic interactions. Thus, it would seem reasonable to suggest the Raman images presented in Fig. 4 indicate the extent of heme aggregation within the cell. The Hb within the cell appears to initially aggregate in the center, with aggregation then continuing toward the periphery of the cell. Areas of dense aggregation are indicated by red in the image, while areas of less dense aggregation are green and the least dense are blue.

3.4 Excitonic Interactions in the Red Cell?

When discussing the origin of Raman enhancement observed in the red cell at 632.8 nm, it is important to note that it is extremely difficult to obtain Raman spectra of Hb solutions at both low and extremely high concentrations (16 to 18 mM) using this excitation wavelength. Long[18] applied 632.8-nm excitation to Hb solutions and reported only weak bands below 600 cm^{-1}. The spectra recorded of single crystals of oxyHb and metHb exhibit bands that are rather broad and featureless compared to their cellular counterparts. The extremely high-quality spectra recorded of single red cells compared to both crystal and solution indicates an extreme ordering of the hemes within the cell. It is hypothesized the enhancement observed when applying 632.8-nm excitation to a single red cell results primarily from excitonic interactions between highly ordered and orientated heme groups within the cell. This enhancement becomes stronger when the heme groups within the cell aggregate in response to photo and/or thermal degradation. The enhancement of many bands, the increase in signal to noise, and the general increase in the background counts is a consequence of the close packing of aggregated hemes enabling energy in the form of an exciton to migrate throughout the aggregated network.

The theory of excitons was developed by Frenkel and Wannier in the 1930s.[19–21] The exciton model is based on the quantum mechanical precept that electronic energy is distributed throughout the aggregate.[22] This arises because interactions between induced transition dipole moments form a superposition of states, resulting in an electronic band of states that enables the movement of electrons throughout the aggregate.[22] In the case of a pure solid, the characterization of vibrational modes of a crystal in terms of amplitudes of individual atomic displacements is not appropriate.[23] Each excited electronic state is "in resonance" with excited states localized at other points in the lattice.[23] Frenkel designated these running states of excitation "excitons" representing particles of excitation.[23] Consequently, true electronic states are linear combinations of these localized excitations each belonging to a wave vector **K** in the reciprocal lattice.[23] Wannier portrayed an exciton as a conduction-band electron and a valence-band

hole, bound together but with a considerable separation, traveling through the crystal in a state of total wave vector **K**.[23] Förster[24] developed a generalized theory of energy transfer (ET) accounting for all types of ET between donor and acceptor models, including biological systems.

The transfer rate for electric dipole or long-range energy transfer known as Förster energy transfer can be written as

$$K_T = \frac{8.8 \times 10^{-25} k^2 \phi_D}{n^4 \tau_D r^6} J, \quad (1)$$

where k is the orientation factor, Φ_D is the donor quantum yield, J represents the overlap integral function between donor emission and the acceptor absorption spectrum, n is the number of molecules, τ_D is the donor lifetime, and r is the distance between the donor and acceptor chromophores.[25] The Förster ET rate has an inverse sixth power dependence of the donor-acceptor separation and has been used to determine intermolecular distances in biological systems.[25] The ET is also directly proportional to the orientation factor k^2, which may vary from 1 to 4 and is defined by the angles between donor and acceptor transition moments.[25] Förster distances of the order 10 to 100 Å are possible depending on the type of chromophore and degree of ordering.[25] An early study by Dervichian, Fouret, and Guinier[26] analyzing small angle x-ray scattering (SAXS) of hemoglobin (Hb) from intact red blood cells showed that the scattering curve displayed a distinct maximum at $2\theta = 0.25$ radians corresponding to an interparticle distance of 62 Å. The authors concluded that the Hb molecules in the cells were not distributed randomly. Perutz[27] showed that the close packing of Hb is an inevitable consequence of the high Hb concentration (34%), because if the molecules were distributed randomly, the interparticle distance would have to be 75 Å and a concentration of 34% could not be achieved. The inter-Hb molecule distance within the red cell is well within the range to enable Förster type long-range excitonic interactions between heme chromophores.

Kasha, Rawls, and El-Bayoumi[28] further developed the exciton theory to explain the systematic spectral changes observed in the Soret band in the absorption spectra of porphyrin arrays, as exemplified by the work of Kim et al. on *meso-meso* covalently linked zinc(II) porphyrins.[29] The UV-visible spectra presented in this study clearly show a broadening and red shift of the Soret band and to a lesser extent the Q bands when comparing a suspension of red cells in saline with isolated Hb in distilled water. On heating the intact red cells, the Soret band becomes broader and both the Soret and Q_0 bands exhibit a distinct red shift. Between 60 and 65 deg the cells lyse, releasing denatured Hb into the surrounding solution. The Soret band is now considerably blue shifted compared to the intact cells. Such broadening and shifting of the Soret band has been interpreted by others to be indicative of excitonic coupling resulting from porphyrin aggregation.[29–31] It should be noted that other contributions can also affect the Soret band width such as inhomogeneous broadening due to conformational heterogeneity, homogenous broadening due to finite life time of the excited state, vibronic coupling with high-frequency nuclear vibrations, and Gaussian broadening due to coupling with a ''bath'' of low-frequency vibrational modes.[32] However, the fact that no broadening of the Soret band was observed in the temperature study of isolated Hb indicates these contributions are minimal at temperatures greater than 45°C.

Akins et al.[22,33–40] demonstrated that the enhancement of Raman scattering is concomitant with the formation of aggregates for a variety of molecules, including cyanine dyes absorbed onto surfaces[34–36,40] and N-protonated porphyrins.[37–39] They advanced the theory of aggregated enhanced Raman scattering (AERS) by incorporating molecular excitonic concepts in a quantum theory analytical expression for aggregated molecules.[33] The enhancement of vibrational modes can be explained in terms of an increase-size effect and near-resonance terms in the polarizability.[22] Akins et al.[22] showed that off-resonance Raman measurements for cyanine dyes in various physical states strongly suggest that molecular aggregation leads to an enhancement in the Raman scattering of intramolecular vibrational modes of the monomeric species and even greater relative enhancement of intermolecular modes directly involved in the formation of the aggregate. In the case of red cells, excitation at 632.8 nm is too far away from the Q_0 ($\sim$570 nm) to be true resonance Raman scattering and possibly too close to be called off-resonance Raman scattering. As mentioned before, we have recorded a Raman excitation profile of crystallized HbA_0 and have shown that the spectrum at 633-nm excitation appears to be independent of resonance or preresonance Raman scattering from the Q_0 band. While we cannot rule out a small electronic transition contributing to the enhancement of numerous bands at 632.8 nm for cells and crystals, it would appear that aggregation enhancement is the dominant mechanism at work.

Further supporting the excitonic hypothesis is the power-dependence study, which clearly shows a nonlinear response for cells at both 4 and 42°C. At the higher temperature, the measured Raman counts for each band are much greater compared to the corresponding measurements at 4°C, and the line appears sigmoidal in shape if the broad baseline is removed prior to the plot. Conversely, for normal Raman enhancement the intensity of Raman bands are directly proportional to the applied power. If excitonic interactions are influencing Raman band intensity, then a nonlinear relationship between power and Raman band intensity is predicted. The nonlinear power-dependence plots reported herein provide evidence supporting the hypothesis that excitonic interactions are responsible for the anomalous enhancement observed in the Raman spectra of red blood cells at 632.8 nm. Moreover, this anomalous enhancement is greater at higher temperatures, indicating that the aggregation and therefore the excitonic interactions are also greater at higher temperatures. Based on these results, it would seem reasonable to conclude that exposing red cells to the higher temperature and/or prolonged laser exposure causes denaturation of the protein leading to heme aggregation. The aggregation enhances the probability of excitonic interactions, and thus also the Raman intensities of many bands along with the background counts.

Goldbeck et al.[41] using Soret circular dichroism (SCD) noted that at high concentrations Hb formed tetramers that had a different SCD profile than those of low concentrations of Hb, which apparently formed dimers. While they could not rule out the possibility that a change in protein conformation or distant heme-aromatic residue interactions was occurring

coincidentally with the excitonic-like feature observed in the spectrum, they did provide evidence that these effects were small and the heme-heme excitonic interaction predicted by Woody[42] was the most compelling explanation.

Recently, Ramser et al.[43] recorded images of an erythrocyte deoxygenated with sodium dithionite using 514-nm excitation and an integration time of 480 s. They also observed an increase in background, which masked any differences between the images of oxygenated and deoxygenated cells. They reasoned the background was due to fluorescence resulting from the thermally activated auto-oxidation of Hb to metHb, and that metHb simply has a higher intrinsic fluorescence than oxyHb.[43] MetHb is in the ferric high-spin ($S = 5/2$) state and therefore cannot bind O_2. The 632.8-nm excitation spectrum of metHb encapsulated in a single living cell prepared and reported as previously described[12] is presented in Fig. 3. This spectrum is very different to spectra recorded after prolonged Raman imaging and/or increasing the temperature. In particular the bands at 1396, 1365, 1249, 972, and 662 cm^{-1} show an increase in relative band intensity at high temperatures and/or after prolonged laser exposure, compared to the analogous bands in the metHb spectrum recorded of the intact cell. The spectrum of metHb is similar to the spectrum recorded of a deoxygenated cell, especially in the spin-state marker band region (1650 to 1500 cm^{-1}). This is not surprising, given that both heme derivatives have a high-spin state configuration resulting in significant translocation of the Fe atom out of the porphyrin plane. The oxygenated cell spectrum is considerably different to metHb and deoxyHb red cell spectra, because in oxyHb the Fe(III) ion is in the low-spin state configuration, thus enabling the Fe atom to translocate into the porphyrin plane. This translocation results in considerable expansion and ruffling of the porphyrin ring and dramatic changes in heme spectra.[44] A marker band for O_2 binding, assigned to v_{10}, appears at 1638 cm^{-1} in the oxygenated red cell. Raman spectra of single crystals of met- and oxyHb show considerable broadening in the 1650- to 1500-cm^{-1} region compared to the isolated cells, indicating a dynamic heme alignment within the single cell. The spectra of the two crystals can be discerned by the appearance of v_{10} at 1638 cm^{-1} in the oxyHb crystal. The unusual enhancement and general increase in background intensity observed at 632.8-nm excitation cannot be due to thermal auto-oxidation of Hb into metHb, otherwise the spectra at these high temperatures or after prolonged laser exposure would resemble metHb. Moreover, the spectra presented in Fig. 8(a) show that the spectral effect observed after partial thermal denaturation could be reversed when the temperature was lowered to 4°C. The spectrum of the cooled cell exhibited a profile consistent with a fully oxygenated cell. Because metHb is incapable of binding O_2, we can rule out the possibility that the spectral effect observed at high temperatures results from the thermal auto-oxidation of Hb to metHb, at least in the case of 632.8-nm excitation.

4   Conclusion

High-quality Raman images of red blood cells are obtained using 632.8-nm excitation. This is achieved by keeping the temperature low (4°C), avoiding prolonged laser exposure (120 s), and reducing the number of multiple images recorded on the same cell (2 in a 90-min period). Prolonged laser ex-

posure results in photoinduced denaturation of the Hb, giving rise to an unusual Raman profile that is characterized by the dramatic enhancement of many bands, an increase in signal-to-noise ratio, and a general increase in background counts. The same effect can be observed when heating the cells to temperatures greater than 42°C. Five bands are identified as marker bands for heme aggregation, namely 1396, 1365, 1248, 972, and 662 cm^{-1}, while two are correlated to O_2 concentration (1638 and 1564 cm^{-1}). The correlation between thermal degradation and the unusual Raman spectra is confirmed by performing Raman measurements as a function of temperature on a population of cells. The spectra at high temperatures closely resemble those recorded after prolonged laser exposure. It is hypothesized that the enhancement is a consequence of Hb aggregation in response to thermal and/or photoinduced denaturation, increasing the probability of excitonic interactions between the hemes. There are five main arguments supporting this hypothesis.

1. The spectra of cells after prolonged laser exposure have a similar relative band enhancement profile to the crystallized deposits of metHb and oxyHb, indicating the Hb in these damaged cells is aggregating or partially crystallizing.

2. The broadening and red shift observed in the Soret band for the red cells compared to the isolated hemoglobin at the higher temperatures may be interpreted as indicative of excitonic interactions in response to heme aggregation.

3. The power-dependence plots of cells in suspensions at 4 and 42°C show a nonlinear curve, with the band enhancement and the nonlinearity much greater at the higher temperature. Nonlinear power dependence is another indicator of excitonic interactions.

4. The signal to noise increases after prolonged laser exposure and at higher temperatures, indicating the number of molecules per unit area has increased, which is a clear indication of aggregation.

5. The interatomic distances between aggregated hemes in the red cell are well within range to enable excitonic interactions.

These points support the hypothesis that excitonic interactions resulting from porphyrin aggregation explain the unusual Raman spectral profile observed at higher temperatures and/or after prolonged laser exposure. The observed effect can be understood in terms of excited state excitonic interactions, whereby the excited state becomes saturated to a point where energy in the form of an exciton can migrate throughout the delocalized environment of the aggregated heme lattice. This additional energy dramatically alters the electronic properties of the chromophore, causing nonlinear optical responses and radical changes in the amplitude of many vibrational modes. It appears that the majority of the Raman cross section of Hb at high temperatures and after prolonged laser exposure can be attributed to this process.

We further postulate that excitonic interactions occur between hemes within the cell when exciting with 632.8-nm excitation, regardless of heme aggregation. There are four arguments to support the hypothesis.

1. It is virtually impossible to record spectra of any quality from Hb solutions irrespective of concentration at 632.8-nm excitation, yet it is relatively simple to record high-quality spectra of red cells with very low power (>1 mW). This indicates a different enhancement mechanism in addition to normal resonance or preresonance Raman scattering occurring on excitation with 632.8-nm excitation.

2. The spectra of single cells are of a much higher quality and better resolved than spectra of their crystallized counterparts, indicating a higher degree of order of heme groups within the cell compared to the crystal. The more ordered the system, the more aligned the chromophores and therefore the higher the probability of excitonic interactions.

3. The Soret band in the absorption spectrum of the red cell is broader and undergoes a 3-nm redshift compared to the spectrum of isolated hemoglobin at low temperature. Such a peak broadening and red shift of the Soret band is indicative of excitonic interactions.

4. The interparticle distance between hemoglobin molecules (62 Å) in the red cell is well in range to enable long-range excitonic coupling mechanisms such as Förster energy transfer to take place.

The results of this study have important implications for realizing the potential biomedical application of Raman imaging and spectroscopy to the analysis of single functional erythrocytes, especially in disorders characterized by heme aggregation reactions including sickle cell disease and malaria.

References

1. T. G. Spiro and X. Y. Li, ''Resonance Raman spectroscopy of metalloporphyrins,'' in *Biological Applications of Raman Spectroscopy*, T. G. Spiro, Ed., pp. 1–38, Wiley, New York (1988).
2. T. G. Spiro and T. C. Streakas, ''Resonance Raman spectra of heme proteins. Effects of oxidation and spin state,'' *J. Am. Chem. Soc.* **96**, 338–345 (1973).
3. H. Brunner, A. Mayer, and H. Sussner, ''Resonance Raman scattering on the haem group of oxy- and deoxyhaemoglobin,'' *J. Mol. Biol.* **70**, 153–156 (1972).
4. G. Fermi, M. F. Perutz, B. Shannan, and R. Fourme, ''The crystal structure of human deoxy hemoglobin at 174 Angstrom resolution,'' *J. Mol. Biol.* **175**, 154–174 (1984).
5. L. Stryer, *Biochemistry*, 3rd. ed., W. H. Freeman and Company, New York (1988).
6. X. Zhao and T. G. Spiro, ''Ultraviolet resonance Raman Spectroscopy of hemoglobin with 200 and 212 nm excitation: H-bonds of tyrosines and prolines,'' *J. Raman Spectrosc.* **29**, 49–55 (1998).
7. G. J. Puppels, H. S. Garritsen, G. M. Segers-Nolten, F. F. De Mul, and J. Greve, ''Raman microscopic approach to the study of human granulocytes,'' *Biophys. J.* **60**, 1046–1056 (1991).
8. B. L. Salmaso, G. J. Puppels, P. J. Caspers, R. Floris, R. Wever, and J. Greve, ''Resonance Raman microspectroscopic characterization of eosinophil peroxidase in human eosinophilic granulocytes,'' *Biophys. J.* **67**, 436–446 (1994).
9. N. M. Sijtsema, A. G. J. Tibbe, I. G. M. J. Segers-Nolten, A. J. Verhoeven, R. S. Weening, J. Greve, and C. Otto, ''Intracellular reactions in single human granulocytes upon phorbol myristate acetate activation using confocal Raman microspectroscopy,'' *Biophys. J.* **78**, 2606–2613 (2000).
10. G. J. Puppels, T. C. Bakker Schut, N. M. Sijtsema, M. Grond, F. Maraboeuf, C. G. de Grauw, C. G. Figdor, and J. Greve, ''Development and application of Raman microspectroscopic and Raman imaging techniques for cell biological studies,'' *J. Mol. Struct.* **347**, 477–483 (1995).
11. K. Ramser, C. Fant, and M. Käll, ''Importance of substrate and photo-induced effects in Raman spectroscopy of single functional erythrocytes,'' *J. Biomed. Opt.* **8**(2), 173–178 (2003).
12. B. R. Wood, B. Tait, and D. McNaughton, ''Micro-Raman characterisation of the R to T state transition of haemoglobin within a single living erythrocyte,'' *Biochim. Biophys. Acta* **1539**, 58–70 (2001).
13. B. R. Wood and D. McNaughton, ''Micro-Raman characterisation of high and low spin haem moieties within a single living erythrocyte,'' *Biopolymers* **67**, 259–262 (2002).
14. C. Piffat, D. Melamed, and T. G. Spiro, ''Ruffling effects on porphyrin vibrations: Normal-mode analysis for nickel octaethyltetraphenylporphine from resonance Raman and IR spectra of isotopomers,'' *J. Phys. Chem.* **97**, 7441–7450 (1993).
15. D. L. Drabkin, ''Spectrophotometric studies XIV. The crystallographic and optical properties of the hemoglobin of man in comparison with those of other species,'' *J. Biol. Chem.* **164**, 703–723 (1946).
16. B. R. Wood and D. McNaughton, ''Raman excitation wavelength investigation of single red blood cells *in vivo*,'' *J. Raman Spectrosc.* **33**, 517–523 (2002).
17. W. J. Williams, E. Beutler, A. Erslev, and M. A. Lichtman, *Hemotology*, 3rd ed., McGraw-Hill, New York (1983).
18. T. V. Long, ''Laser-Raman spectroscopy of bio-inorganic molecules,'' *Univ. Ill. Bull.* **67**, 59–61 (1969).
19. J. Frenkel, ''On the transformation of light into heat in solids. I,'' *Phys. Rev.* **37**, 17–44 (1931).
20. J. Frenkel, ''On the transformation of light into heat in solids. II,'' *Phys. Rev.* **37**, 1276–1293 (1931).
21. G. H. Wannier, ''The structure of electronic excitation levels in insulating crystals,'' *Phys. Rev.* **52**, 191–197 (1937).
22. D. L. Akins, S. Özcelik, H. R. Zhu, and C. Guo, ''Aggregation-enhanced Raman scattering of a cyanine dye in homogenous solution,'' *J. Phys. Chem. A* **101**, 3251–3259 (1997).
23. R. S. Knox, *Theory of Excitons*, Academic Press, New York (1963).
24. Th. Förster, ''Zwischenmolekulare energicwanderun und floureszenz,'' *Ann. Phys. (Leipzig)* **2**, 55–75 (1948).
25. J. Eisinger and R. E. Dale, ''What has energy transfer done for biochemistry lately?'' in *Excited States of Biological Molecules*, J. B. Birks, Ed., pp. 579–590, John Wiley and Sons, London (1974).
26. D. G. Dervichian, G. Fournet, and A. Guinier, ''Mise en evidence d'une structure submicroscopique dans les globules rouges par la diffusion des rayons X aux petits angles,'' *C. R. Acad. Sci. Paris* **224**, 1848–1850 (1947).
27. M. F. Perutz, ''Submicroscopic structure of the red cell,'' *Nature (London)* **161**, 204–206 (1948).
28. M. Kasha, H. R. Rawls, and M. A. El-Bayoumi, ''The exciton model in molecular spectroscopy,'' *Pure Appl. Chem.* **11**, 371–392 (1965).
29. Y. H. Kim, D. H. Jeong, D. Kim, S. C. Jeoung, H. S. Cho, S. K. Kim, N. Aratani, and A. Osuka, ''Photophysical properties of long rodlike *meso-meso*-linked Zinc (II) porphyrins investigated by time-resolved laser spectroscopic methods,'' *J. Am. Chem. Soc.* **123**, 76–86 (2001).
30. D. M. Chen, Y. H. Zhang, T. J. He, and F. C. Liu, ''Raman and UV-visible absorption spectra of ion-paired aggregates of copper porphyrins,'' *Spectrochim. Acta* **58**, 2291–2297 (2002).
31. A. A. Bhuiyan, J. Seth, N. Yoshida, A. Osuka, and D. F. Bocian, ''Resonance Raman characterisation of excitonically coupled *meso,meso*-linked porphyrin arrays,'' *J. Phys. Chem. B* **104**, 10757–10764 (2000).
32. M. Leone, A. Cupane, and L. Cordone, ''Low temperature optical spectroscopy of low-spin hemeproteins,'' *Eur. Biophys. J.* **24**, 117–124 (1996).
33. D. L. Akins, ''Theory of Raman scattering by aggregated molecules,'' *J. Phys. Chem.* **90**, 1530–1534 (1986).
34. D. L. Akins and J. W. Macklin, ''Dependence of Raman scattering by aggregated 2,2′-cyanine on pH and excitation wavelength,'' *J. Phys. Chem.* **93**, 5999–6007 (1989).
35. D. L. Akins, J. W. Macklin, L. A. Parker, and H. R. Zhu, ''Raman

excitation spectra of aggregate modes of 2,2′-cyanine," *Chem. Phys. Lett.* **169**, 564–568 (1990).

36. D. L. Akins, J. W. Macklin, and H. R. Zhu, "Fourier transform Raman spectra and the structure of adsorbed 2,2′-cyanine," *J. Phys. Chem.* **95**, 793–798 (1991).

37. D. L. Akins, S. Özcelik, H. R. Zhu, and C. Guo, "Fluorescence decay kinetics and structure of aggregated tetrakis(p-sulphonatophenyl porphyrin," *J. Phys. Chem.* **100**, 14390–14396 (1996).

38. D. L. Akins, H. R. Zhu, and C. Guo, "Absorption and Raman scattering by aggregated *meso*-tetrakis (p-sulphonatophenyl) porphine," *J. Phys. Chem.* **98**, 3612–3618 (1994).

39. D. L. Akins, H. R. Zhu, and C. Guo, "Aggregation of tetraaryl-substituted porphyrins in homogenous solution," *J. Phys. Chem.* **100**, 5420–5425 (1996).

40. D. L. Akins, Y. H. Zhuang, H. R. Zhu, and J. Q. Liu, "Raman excitation spectra of exciton-phonon modes of aggregated 2,2′-cyanine using an internal Raman standard," *J. Phys. Chem.* **98**, 1068–1072 (1994).

41. R. A. Goldbeck, L. Sagle, D. B. Kim-Shapiro, V. Flores, and D. S. Kliger, "Evidence for heme-heme excitonic coupling in the Soret circular dichroism of hemoglobin," *Biochem. Biophys. Res. Commun.* **235**, 610–614 (1997).

42. R. W. Woody, *Optical Properties and Structure of Tetrapyrroles*, G. Blauer and H. Sund, Eds., pp. 239–256, Walter de Gryter, New York (1985).

43. K. Ramser, E. J. Bjerneld, C. Fant, and M. Kall, "Raman imaging and spectroscopy of single functional erythrocytes: a feasibility study," *Proc. SPIE* **4614**, 20–27 (2002).

44. T. G. Spiro, J. D. Stong, and P. Stein, "Porphyrin core expansion and doming in heme proteins. New evidence from resonance Raman spectra of six-coordinate high-spin iron (III) hemes," *J. Am. Chem. Soc.* **101**, 2648–2655 (1979).